Journal of Nanoparticle Research (2006) 8:783–796
DOI 10.1007/s11051-005-9029-6

Sensing low concentrations of CO using flame-spray-made Pt/SnO_2 nanoparticles

L. Mädler[1,4,*], T. Sahm[2], A. Gurlo[2], J.-D. Grunwaldt[3], N. Barsan[2], U. Weimar[2] and S.E. Pratsinis[1]
[1]*Particle Technology Laboratory, Swiss Federal Institute of Technology (ETH) Zurich, Sonneggstrasse 3, CH-8092, Zürich, Switzerland;* [2]*Institute of Physical and Theoretical Chemistry, University of Tübingen, Auf der Morgenstelle 8, D-72076, Tübingen, Germany;* [3]*Department of Chemistry and Applied Biosciences, Swiss Federal Institute of Technology (ETH) Zurich, Hönggerberg, CH-8093, Zürich, Switzerland;* [4]*Department of Chemical Engineering, University of California, Los Angeles, 5531-G Boelter Hall, Los Angeles, CA, 90095, USA; *Author for correspondence (Tel.: +310-825-9926; Fax: +310-206-4107; E-mail: lutz@seas.ucla.edu)*

Received 6 April 2005; accepted in revised form 29 July 2005

Key words: gas sensor, CO detection, flame spray pyrolysis, tin dioxide nanoparticles, platinum functionalization, XPS/EXAFS, combustion

Abstract

Tin dioxide nanoparticles of different sizes and platinum doping contents were synthesized in one step using the flame spray pyrolysis (FSP) technique. The particles were used to fabricate semiconducting gas sensors for low level CO detection, i.e. with a CO gas concentration as low as 5 ppm in the absence and presence of water. Post treatment of the SnO_2 nanoparticles was not needed enabling the investigation of the metal oxide particle size effect. Gas sensors based on tin dioxide with a primary particle size of 10 nm showed signals one order of magnitude higher than the ones corresponding to the primary particle size of 330 nm. *In situ* platinum functionalization of the SnO_2 during FSP synthesis resulted in higher sensor responses for the 0.2 wt% Pt-content than for the 2.0 wt% Pt. The effect is mainly attributed to catalytic consumption of CO and to the associated reduced sensor response. Pure and functionalized tin dioxide nanoparticles have been characterized by Brunauer, Emmett and Teller (BET) surface area determination, X-ray diffraction (XRD), high resolution transmission electron microscopy (HRTEM) and scanning transmission electron microscopy (STEM) while the platinum oxidation state and dispersion have been investigated by X-ray photoelectron spectroscopy (XPS) and extended X-ray absorption fine structure (EXAFS). The sensors showed high stability (up to 20 days) and are suitable for low level CO detection: <10 ppm according to European and 50 ppm according to US legislation, respectively.

Introduction

Gas sensors based on semiconducting metal oxides are one of the most investigated group of gas sensors (Pearce et al., 2004). For them, the conductance G or electrical resistance R is monitored as a function of the concentration of target gases and subjected to further data treatment and processing. SnO_2-based sensors are the best-understood prototype of oxide-based gas sensors and, in particular, have been used widely in gas sensing under atmospheric conditions (Barsan et al., 1999; Barsan & Weimar 2003; Eranna et al., 2004).

One of today's challenges in carbon monoxide (CO) monitoring is the low concentration range (i.e. below 50 ppm) because of the fact that it is a toxic

gas accompanying nearly all combustion processes. The US Occupational Safety and Health Administration (OSHA) has set a general industry Permissible Exposure Level (PEL) for CO of 50 ppm averaged over an 8 h work shift (http://www.osha.com). The American Conference of Governmental Industrial Hygienists (ACGIH), a private professional organization, has adopted a threshold limit value (TLV) of 25 ppm. In Europe, the limit value of CO (maximum daily 8 h mean) for the protection of human health to be met in 2005 is set at 10 mg/m^3 ($\approx$8.75 ppm) (EN, 2000). At present, for example, in Germany, there are two kinds of occupational exposure limits (OELs) for air in the workplace: Technische Richtkonzentrationen (TRKs), which are technical guidance concentrations, and Maximale Arbeitsplatz Konzentrationen (MAKs), which give the maximum concentration of a chemical substance in the workplace (the MAK-values are daily 8 h time-weighed average values and apply to healthy adults). In Germany the MAK value for CO is set at 30 ppm.

For CO detection on metal-oxide (i.e. SnO_2) based gas sensors, it is well known and generally accepted that the CO reacts with the adsorbed oxygen ions (like O_2^- or O^-) getting oxidized to CO_2 and the released electrons (sensing step) can therefore return to the conduction band (CB) according to the scheme:

$$CO_{(gas)} + O^-_{(s)} \rightarrow CO_{2\,(gas)} + e\,(CB)$$

Water has a similar reaction path way with the absorbed oxygen radical and therefore the effect of CO is often shielded by water (Sahm et al., 2005). To enhance the sensing properties, SnO_2 is often functionalized with different noble metals (i.e. usually Pd, Pt, Au). In general, this decreases the response and recovery times, and increases the sensitivity, selectivity, reproducibility and stability of the sensors (Yamazoe, 1991; Sweizer-Berberich et al., 1996). However, in each particular case – depending on the amount, chemical state, aggregation and localization of the atoms – the noble metal can influence the sensing properties in completely different manner; no generalization can be made even for the same base material (i.e. SnO_2) (Matsushima et al., 1988; Yamazoe, 1991; Gaidi et al., 1998; Kappler et al., 1998; Matko et al., 1999, 2002; Cabot et al., 2000, 2001, 2002; Dieguez et al., 2000). Usually, surface functionalization leads to an improvement of the sensing properties, while the doping with higher concentrations results in materials with poorer sensing properties (Grandjean et al., 2004). Moreover, the situation will be different if the noble metal forms isolated metallic nanoparticles of a few nanometers (''metallic clusters'') or is getting oxidized and diffusing into the lattice of base material (SnO_2) forming solid-solutions (this is especially favorable for platinum because PtO_2 has the crystalline structure of rutile – the same as cassiterite structure of SnO_2).

The production of homogenous SnO_2 nanoparticles by flame spray pyrolysis (FSP) for gas sensing has been demonstrated successfully for sensing of NO_2 and propanal (Sahm et al., 2004). In general, FSP has the ability to control particle size, produce highly single crystalline nanoparticles (Mädler et al., 2002a), and functionalize metal oxides within on step, often called *in situ*, with noble metals (Mädler et al., 2003; Strobel et al., 2003). Therefore, FSP is well suited to address the effects of tin dioxide nanoparticle properties such as size, crystallinity and platinum functionalization with regard to gas sensing performance and in particular CO detection. The resulting high external surface area, high noble metal dispersion and the absence of a powder post-calcinations step are further advantages of the FSP with regard to sensor manufacture.

Experimental

Nanoparticle synthesis

An aerosol reactor was used to produce SnO_2 and Pt/SnO_2 nanoparticles by FSP (Mädler et al., 2002b). The liquid precursor was prepared by diluting tin(II) 2-ethylhexanoic acid (Sigma-Aldrich, purity $>98\%$) in toluene (Fluka, purity $>99.5\%$) to obtain a 0.5 M precursor solution. For Pt/SnO_2 synthesis, appropriate amounts of platinum acetylacetonate ($Pt(acac)_2$, Strem, purity $>98\%$) were added to the solution to obtain a platinum loading of 0.0, 0.2 and 2.0 wt%, respectively. The liquid precursor was fed by a syringe pump (Inotech R232) with a constant feed rate of 5 and 8 ml/min through a capillary of an outside-mixing two-phase nozzle. The liquid was dispersed into fine droplets with 3 and 5 l/min oxygen (Pan Gas, 99.95%) maintaining a pressure

drop of 1.5 bar at the nozzle exit. All gas flow rates were controlled by calibrated mass flow controllers (Bronkhorst). In particular, the flame spray was operated at two different sets of flow rates: 5 ml/min liquid precursor feed rate with 5 l/min oxygen dispersion gas (defined as 5/5) and 8 ml/min liquid precursor feed rate with 3 l/min oxygen dispersion gas (defined as 8/3). The liquid spray was ignited by a premixed methane/oxygen (1.5 l/min/3.2 l/min, respectively) flame ring surrounding the nozzle exit (Mädler et al., 2002b). A sintered metal plate ring (8 mm wide, at inner radius of 9 mm from the center of nozzle) issued additional 5 l/min of oxygen as a shield gas. The powder was collected with the aid of a vacuum pump on a glass fiber filter (GF/D Whatman, 257 mm in diameter). During the experiment, the filter was placed in a water-cooled holder, 400 mm above the nozzle, keeping the off-gas temperature below 200°C.

Powder characterization

X-ray diffraction patterns were recorded with Bruker AXS D8 Advance (40 kV, 40 mA) and used to obtain the crystallite size (d_{XRD}) based on the fundamental parameter approach and the Rietveld method (Cheary & Coelho, 1998) with the structural parameters of cassiterite (ICSD Coll. Code: 084576; Bolzan et al., 1997). A linear background was used when matching the XRD patterns while microstrain was not considered. The BET powder specific surface area (SSA), was measured by nitrogen adsorption at 77 K (Micromeritics Gemini 2375) after degassing the sample, at least, for 1 h at 150°C in nitrogen. Assuming monodisperse spherical primary particles within an aggregate, the equivalent average primary particle diameter d_{BET} was calculated by $d_{BET} = 6/(SSA\ \rho_p)$, where ρ_p is the density of SnO_2 (6.85 g/cm^3). Transmission electron microscopy analysis was carried out with a Phillips CM30ST microscope (LaB_6 cathode, 300 kV). Scanning transmission electron microscopy (STEM) images were obtained with a high-angle annular dark-field (HAADF) detector (Z contrast).

X-ray photoelectron spectroscopy (XPS) measurements were performed on a Leybold Heraeus LHS11 MCD instrument using MgKα (1253.6 eV) radiation (Grunwaldt et al., 1997). The analyzer was operated at 150 eV pass energy. The sample was fixed on a sample holder on top of a graphite foil and transferred to a load lock chamber where it was evacuated at room temperature for 2 h down to 10^{-6} mbar. Finally, it was transferred to the analysis chamber at a typical pressure of 10^{-9} mbar. For quantification of the composition the following peaks were used: O1s, C1s, Pt4f (both $Pt4f_{5/2}$ and $Pt4f_{7/2}$), and $Sn3d_{5/2}$. The Shirley-type background subtraction and quantification of the surface concentration were performed using the SPECSLAB software package (SPECSLAB, Program software for XPS, ISS, and UPS, Specs., Berlin, Germany). Sensitivity factors used for calculation of the surface composition were taken from the SPECSLAB program (SPECSLAB, Program software for XPS, ISS, and UPS, Specs., Berlin, Germany). The spectra were not corrected for the shift since only for the SnO_2 sample partial charging was observed. The 2.0 wt% Pt/SnO_2 sample was not charged at all, while the 0.2 wt% Pt/SnO_2 sample showed a small fraction (ca. 5%) that was charged. Note that the Pt to Sn surface ratio was determined by acquiring separate spectra over about 24 h in case of 0.2 wt% Pt/SnO_2 to obtain a sufficient signal-to-noise ratio.

In order to gain further insight into the structure of the Pt dopants, additionally, EXAFS spectra at the Pt L_3-edge were taken of as-prepared powder 0.2 wt% Pt/SnO_2 and 2.0 wt% Pt/SnO_2 samples. Note that the low loading of Pt on a strongly X-ray absorbing support requires detection in the fluorescence mode (Iwasawa, 1996; Kappen et al., 2002). This was achieved with a 5-element solid state detector (Canberra) at ANKA-XAS in Karlsruhe (Forschungszentrum Karlsruhe, Germany). The as-prepared samples were monitored after pressing them to self supporting discs/pellets. Data were collected between 11.45 and 12.3 keV in the step-scanning mode using a Si(111) double crystal for monochromatization of the X-rays (typically detuned to 60% of the intensity to remove higher harmonics). The raw data were energy-calibrated with the Pt metal foil (Pt L_3-edge), background corrected, and normalized using the WINXAS 3.1 program package (Ressler, 1998). Fourier transformation was applied in the range 2.5–12 Å^{-1}.

Sensor characterization

DC electrical measurements (sensor tests) have been performed to monitor the response to CO in synthetic air with 0% (dry), 10% and 50% relative

humidity (r.h.) at 20°C. The sensing layers were fabricated by classical thick film deposition technology (i.e. screen printing or drop-coating, see Sahm et al., submitted) of a suspension of the FSP-made nanoparticles on the alumina substrates with interdigitated Pt electrodes on the front side and a heater on the back side (Barsan & Weimar, 2003). For the comparison tests, commercially available SnO_2 powder (Sigma-Aldrich, mesh 325, $d \approx 330$ nm) was also used. After the deposition of the sensing layer, the as-obtained sensors were fired in air in a moving belt oven (Centrotherm Centronic DO 1600-60-D5) with four individually operated heating zones. The velocity of the moving belt was adjusted to allow the sensors to stay in the maximum temperature zone (actually, at 500°C) for 10 min.

The conventional sensor tests were performed with a set of four sensors placed in a teflon-made test chamber and operated in the same conditions. The operating temperature of the sensors was adjusted between 200 and 400°C for individual sensor tests. A computer driven gas-mixing system provided the analyte gas for sensing evaluation (Kappler, 2001). CO catalytic conversion measurements have been performed for 0.2 and 2.0 wt% Pt doped sensors by the use of eight identical sensors, respectively. These sensors have been placed into two test-chambers that were connected in series. The first one contained a single sensor, whereas in the second one seven sensors were arranged along the gas flow with always two sensors opposing each other. For stability tests, a set of four sensors (two sensors with 0 wt% Pt and two with 0.2 wt% Pt) has been exposed to a test cycle of three different CO concentrations (10, 240 and 50 ppm) repeating every second day for a period of 20 days. The sensing properties were assessed through sensor signal S, reported as the resistance ratio R_{air}/R_{gas}, where R_{gas} and R_{air} denote the sensors' resistances in the presence and absence of CO, respectively (please note that the sensor signal has units of ohm/ohm).

Results and discussion

Effect of nanoparticle size on sensing properties

Characterization of tin dioxide nanoparticles

Pure SnO_2 nanoparticles were produced at two conditions: flame 5/5 or 8/3. These conditions correspond to relatively low temperatures and dilute aerosols or high temperatures and dense aerosols, respectively (Mädler & Pratsinis, 2002). In general, increasing the ratio of the precursor liquid to dispersion gas flow rate increased the average primary particle size as determined by BET from about 9.9 (88.1 m^2/g) to 19.4 nm (45.2 m^2/g). Figure 1 shows the corresponding X-ray diffraction patterns of these powders which were present in the cassiterite phase of tin dioxide. Applying fundamental parameter and Rietveld analysis on SnO_2 (Sahm et al., 2004) resulted in average crystallite sizes of 10.7 and 19.8 nm for the particles made with flames 5/5 and 8/3, respectively. The excellent agreement between the corresponding BET and XRD average size of the powders indicates the presence of monocrystalline particles. The high crystallinity and the presence of single crystalline primary particles was confirmed by the high resolution transmission electron analysis and the corresponding electron diffraction pattern of a powder produced with the 5/5 configuration (figure 2). Furthermore, the average size of the individual primary particles in the HRTEM image is in good qualitative agreement with the reported d_{BET} and d_{XRD}. The precise control of

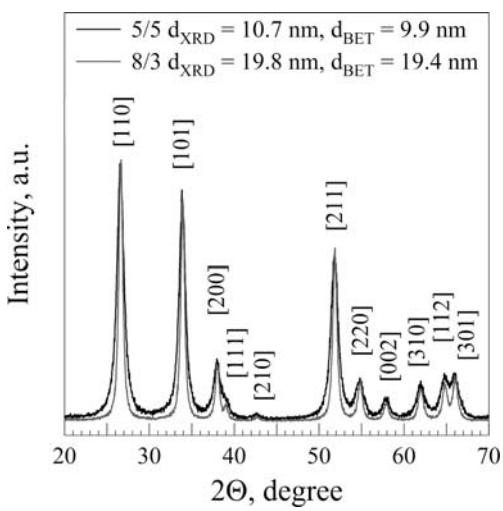

Figure 1. X-ray diffraction patterns of pure SnO_2 powders made at different flame conditions. Increasing the precursor to oxygen feed ratio increases the tin dioxide grain size and therefore narrows the peak width. Excellent agreement between XRD and BET analysis indicates the presence of monocrystalline SnO_2 particles. Numbers in brackets identify lattice planes.

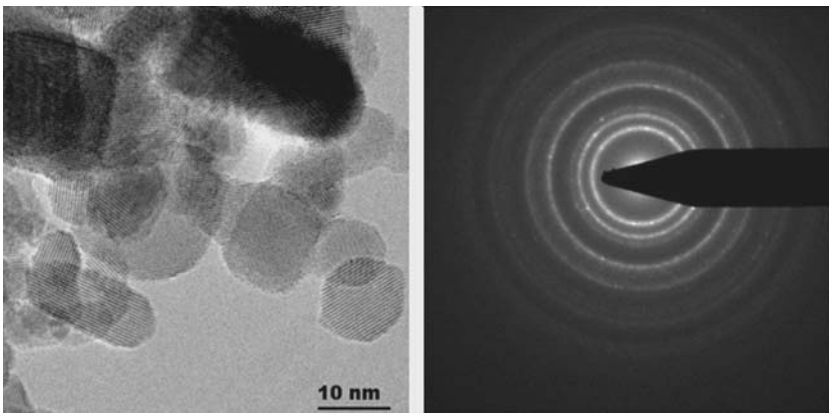

Figure 2. High resolution TEM and the electron diffraction pattern of particles produced in the flame 5/5. The tin dioxide powder shows high crystallinity and individual particles are mostly monocrystalline.

particle size and the high crystallinity of the FSP products have been demonstrated previously for various single oxide powders such as silica, ceria, bismuth oxide and zinc oxide (Mädler et al., 2002a, b; Mädler & Pratsinis, 2002; Tani et al., 2002).

Characterization of sensors made from pure tin dioxide

For benchmarking reason, sensors based on sensing materials obtained by FSP were compared to sensors based on commercially available tin dioxide (Figure 3). For the case of a commercial powder from Sigma-Aldrich, with an average diameter of 330 nm, one records two orders of magnitude lower total resistance; this might be an advantage in practical applications because of the possibility of using simple read out electronics. However, the sensor signal (at 500 ppm; this high CO concentration was chosen due to the low sensitivity of sensors based on commercial SnO_2 powder) is drastically increased for the FSP materials with primary particle size 10 nm (where it reaches a maximum). The reasons for the increase, corresponding to the lowest grain size value, could be: the higher specific surface area within the sensing layer, the larger influence of the surface phenomena (the relative increase of depletion layer in comparison with the particle size itself), a different surface microstructure that induces a different reactivity, a different concentration of bulk defects that results in a different availability of free charge carriers, etc.

A detailed study of the grain size effects on sensors with reasonable good sensor response is limited at the moment; the fabrication of particles smaller than 10 nm is possible by FSP but their processing into sensing layers by conventional film deposition techniques (here screen printing) is very difficult. In general, the effect of grain size on sensing performance is still under debate since the work and models of Xu et al. (1991) and Rothschild and Komem (2004). It is difficult to compare results and estimate the influence of the particle size on gas sensing properties because other parameters which influence the electrical properties

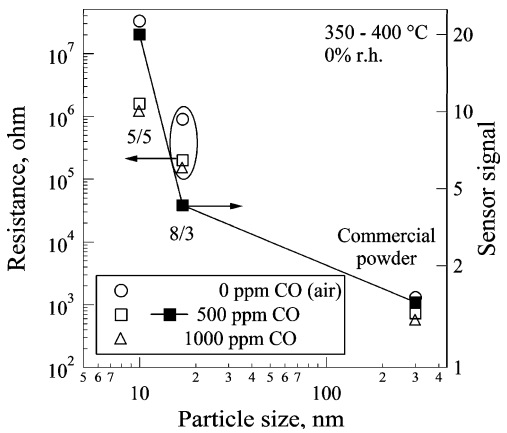

Figure 3. Resistance (left axis, open symbols) and sensor signal (right axis, filled squares) for pure SnO_2 sensors of different particle sizes. With increasing particle diameter the resistance in air (○), in 500 ppm CO (□) and in 1000 ppm CO (△) decreases. Also the sensor signal for 500 ppm CO (■) decreases with increasing particle size. The measurements have been performed on drop-coated sensors at 350°C (flame 8/3 and commercial powders) and screen-printed sensors at 400°C (flame 5/5 powder) in dry air.

of SnO_2 gas sensor were not reported in most of the previous experiments. The change in grain size was for example accompanied by variations in other microstructural features; therefore the conclusion about size dependence of gas sensitivity could be misleading.

As the highest sensor signals came from the smallest tin dioxide grain size (flame 5/5) these particles were investigated in detail. Figure 4 presents the sensor response when tested at very low CO concentrations in the range from 5 to 50 ppm at different operating temperatures. In general, the sensor shows high signal values and its performance is best at an operating temperature of 300°C.

Effect of SnO_2 nanoparticle functionalization with Pt

Characterization of platinum doping

Platinum doping of tin dioxide is performed *in situ* with the FSP process by dissolving the corresponding components in the liquid precursor/fuel. The first *in situ* functionalization of metal oxides with platinum in a flame process was demonstrated by Johannessen and Koutsopoulos (2002) while the highly efficient platinum doping by the FSP process was outlined for a Pt/Al_2O_3 catalyst by Strobel et al. (2003). In their study it was additionally demonstrated that platinum is present as highly dispersed clusters and the nominal mass loading is preserved in the final product.

Figure 5 shows a scanning transmission electron microscopy (STEM) image in Z-contrast of tin dioxide with a 2.0 wt% platinum doping made with at the flame 5/5. The inherent Z-contrast difference between tin and platinum is not very high, resulting in a rather blurred image. However, the picture reveals clearly the absence of particle inhomogeneities and proofs the presence of the platinum by the corresponding EDX analysis of

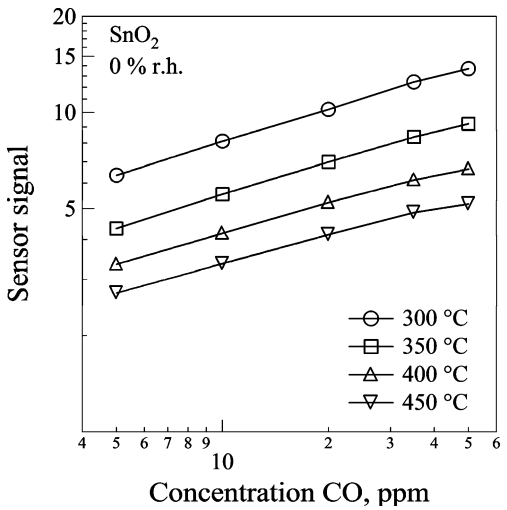

Figure 4. Temperature dependence of the sensor signal of pure SnO_2 sensors for different CO concentrations in dry air. A power law dependence has been observed for all examined temperatures.

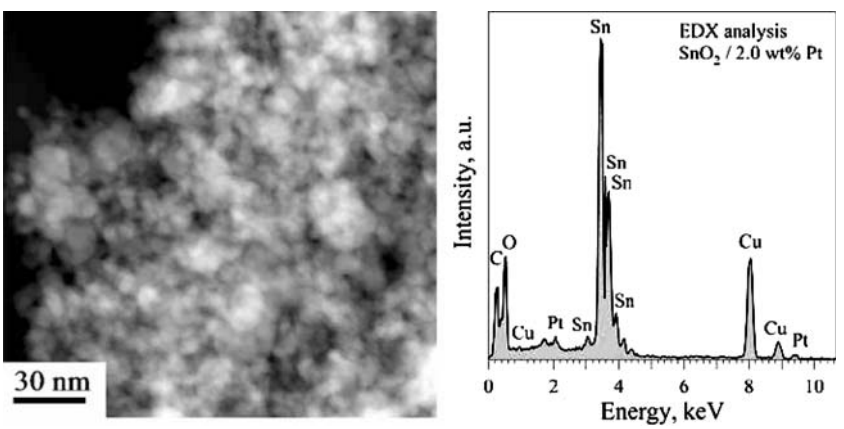

Figure 5. Left: Scanning transmission electron microscopy (STEM) image in Z-contrast of tin dioxide with a 2.0 wt% platinum doping (flame 5/5) indicating the absence of particle inhomogeneities. Right: Corresponding EDX analysis. The presence of the copper and carbon signals in the EDX spectrum resulted from the carbon coated copper TEM grid used.

that section (Figure 4). The presence of the copper and carbon signals in the EDX spectrum resulted from the carbon coated copper TEM grid used.

Figure 6 shows the tin dioxide XRD patterns for different platinum loadings of 0.0, 0.2 and 2.0 wt% (flame 5/5). The highly crystalline cassiterite structure and the tin dioxide crystallite size were not influenced by the addition of platinum resulting in an unchanged BET surface area. The employed small platinum loadings at these FSP conditions could not be detected by XRD indicating the absence of large (10 nm and larger) crystalline platinum particles. Detailed information about the platinum can only be obtained from surface sensitive or element-specific analysis methods. The XPS analysis resulted in a theoretical Pt/Sn ratio of 0.016:1 in 2.0 wt% Pt/SnO_2 which is somewhat lower than the observed 0.006:1 ratio but may be explained with incorporation of Pt into the SnO_2-lattice (Table 1). Note also that the relative surface composition is more straightforward to interpret than the absolute surface composition. The relative Pt/Sn ratio evidences that the 0.2 wt% Pt/SnO_2 sample is better dispersed (Table 1). Interestingly, both platinum doped samples show hardly any charging in XPS, while the SnO_2 sample does (Table 1).

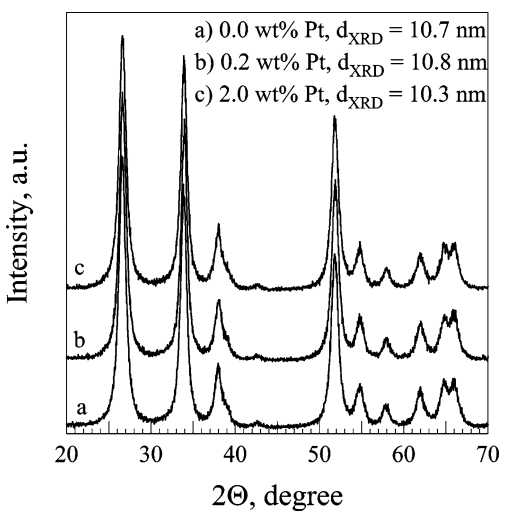

Figure 6. Tin oxide crystal structure for platinum loadings of 0.0, 0.2 and 2.0 wt% (flame 5/5). The highly crystalline cassiterite structure and the tin oxide crystallite size were not influenced by the addition of platinum. The small platinum loadings of 0.2 and 2.0 wt% cannot be detected (e.g. at about 46°).

The binding energies observed for tin dioxide are typical for those reported for Sn^{IV} (Muilenberg, 1979). The analysis of the Pt 4f peaks shows only one dominant species which is significantly higher in binding energy than that reported for Pt^0. It has been reported that Pt foil has Pt $4f_{7/2}$ and Pt $4f_{5/2}$ peaks at 70.7–70.9 and 74.0–74.15 eV, respectively (Kim et al., 1971; Muilenberg, 1979; Yang et al., 1997). The Pt $4f_{5/2}$ peaks of Pt^{2+} and Pt^{4+} species are located around 72.5 and 73.5–74.0 eV, respectively (Kappler et al., 1998; Muilenberg, 1979). The Pt 4f peaks observed in the two Pt-doped SnO_2 samples are closely related to Pt^{2+}-species. However, the slight shift to lower binding energies may indicate some reduced species or loss of oxygen. No PtO_2 species as in Dieguez et al. (2000) were detected. Only one dominant species was found and a partially reduced Pt-species may be correlated to the semiconducting properties of SnO_2 (note also that charging was observed). Furthermore, pumping in ultrahigh vacuum may result in a partial reduction of the platinum, leading to smaller shifts than expected for Pt^{2+}. Therefore, EXAFS spectra were recorded under ambient conditions without evacuation (see results further below).

At normal conditions under air, Pt is in oxidized state as revealed both by fl-XANES (X-ray Absorption Near Edge Structure in the fluorescence mode) and by fl-EXAFS (Figure 7) for the sensors made from FSP nanoparticles. The strong whiteline in XANES indicates that the Pt-species are well oxidized in the SnO_2 lattice (Gaidi et al., 1998, 2000; Bazin et al., 1999; Kappen et al., 2002). Hence, these results show that already under vacuum or during X-ray irradiation in the XPS chamber loss of oxygen occurs leading to slightly shifted Pt 4f-peaks in XPS. Also the Fourier-transformed EXAFS data (Figure 7b) show that platinum is in oxidized state in ambient air. Further, both XANES and EXAFS indicate a high dispersion of the Pt inside the support since Pt is strongly oxidized (Figure 7a) and hardly any Pt backscatters are found in the fl-EXAFS data of as-prepared Pt/SnO_2 powders (Figure 7b). These results are similar to recent data by *in situ* EXAFS on 3.0–12.0 wt% Pt-doped SnO_2 prepared by submicronic aerosol pyrolysis (Gaidi et al., 1998, 2000). However, no Pt-aggregates are found in our as-prepared samples.

Table 1. Surface composition determined from XPS-analysis and the binding energies of the different peaks

Sample	SnO_2	0.2 wt% Pt–SnO_2	2.0 wt% Pt–SnO_2
Shift	6 eV for most of the sample	No shift[a]	No shift
C1s [at%]	22.7	41.3[b]	29.3[b]
O1s [at%]	58.6	42.6	51.5
$Sn3d_{5/2}$ [at%]	18.6	16.0	19.0
Pt 4f [at%]	–	0.02	0.1
Pt/Sn-ratio[c]	–	0.0010:1	0.0058:1
O1s/eV	537.9	531.0	531.1
Pt $4f_{7/2}$/eV	–	71.9	72.2
Pt $4f_{5/2}$/eV		75.5	75.4
$Sn3d_{5/2}$/eV	487.1 (19.5%)	487.0 (57.1%)	487.1
	493.9 (39.7)		
$Sn3d_{3/2}$/eV	495.5 (12.9%)	495.4 (40.5%)	495.5
	502.3 (27.8%)	502.3 (2.4%)[d]	

[a]For a small fraction some shift was found (see at the $Sn3d_{3/2}$ peak).
[b]Note that the carbon stems from graphite below the sample (small sample size).
[c]Determined by additional longer recording time of the Pt 4f and Sn 3d region.
[d]Note that this small fraction of $Sn3d_{3/2}$ is due to partial charging of the sample which amounts to about 5%.

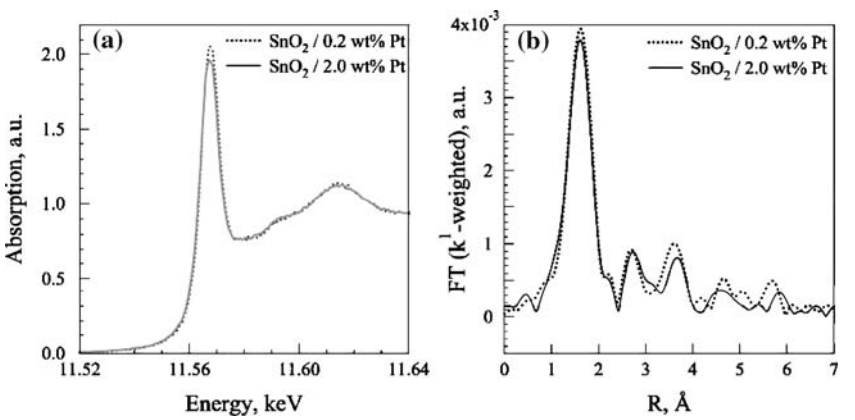

Figure 7. (a) XAS-spectra taken in the fluorescence mode around the Pt L_3-edge of 0.2 wt% Pt/SnO_2 and 2.0 wt% Pt/SnO_2 and (b) corresponding Fourier transformed spectra (not phase corrected).

Characterization of sensor made from platinum doped tin dioxide

Figure 8 shows the response to small concentrations of CO (5–50 ppm) of sensors which had been *in situ* functionalized with 0.2 (on the left) and 2.0 wt% platinum (on the right). Doping the tin dioxide with 0.2 wt% platinum results in a much steeper calibration curve and the highest sensor signals compared to pure tin dioxide (see Figure 4). The higher sensor signal and especially the higher sensitivity (i.e. the steeper response curve) increase sensor performance. Also in the case of platinum doping the best performance is achieved at a sensor operating temperature of 300°C. However, the situation is completely different when adding more platinum. Here, 2.0 wt% reduces the performance drastically and only at the highest concentration of 50 ppm the sensor starts to respond to CO. Note, that these tests were performed with a set of four sensors placed in a teflon-made chamber.

This is in agreement with the general findings on the influence of Pt-doping (i.e. functionalization) on the CO sensing properties of SnO_2. The low concentrations of platinum increases the signals to CO whereas increase in platinum concentration leads to the decrease in sensing properties. This was reported also for the sol-gel (or precipitated)

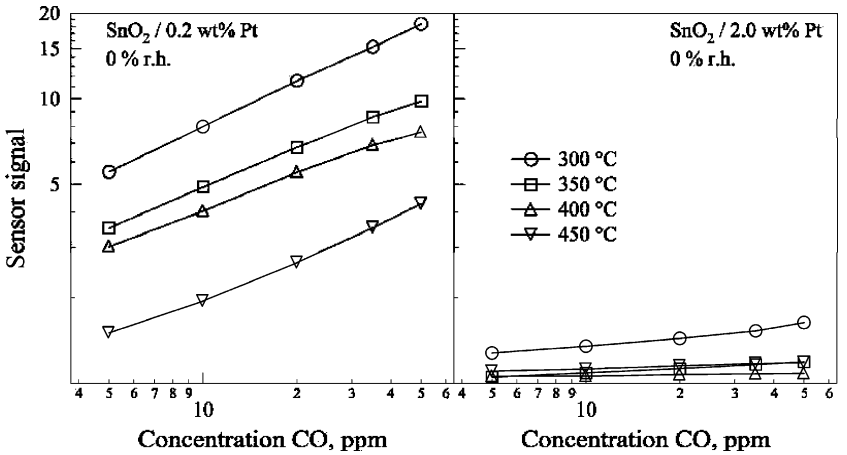

Figure 8. Signal of SnO_2 sensors doped with 0.2 wt% Pt (left) and 2.0 wt% Pt (right) as a function of CO concentrations in dry air at four temperatures. The signal increases with increasing CO concentration and decreasing sensor temperature. A power law dependence has been observed for all examined temperatures.

SnO_2 with 0.2 wt% (Pt/Sn ratio is 0.0016) and 2.0 wt% Pt (Pt/Sn ratio: 0.016). In this case the platinum was introduced either by impregnation of the pre-calcined SnO_2 with a platinum chloride precursor or by precipitating it in solution before the thermal treatment (Kappler et al., 1998, 2001; Cabot et al., 2000, 2001, 2002; Cabot, 2004). Similar findings were reported for pyrosol co-deposited Pt/SnO_2 (Pt/Sn ratio: between 0.019 and 0.200) (Matko et al., 2002). In the wet phase method the 0.2 wt% Pt doping increases significantly the sensor signal to CO both in dry and especially in humid (50% r.h at 20°C) air, in contrast to 3.0 wt% Pt which decreases this property (Kappler, 2001). In both cases (for 0.2 and 2.0%) for the wet phase method Pt was found to be present in oxidized form (as Pt^{2+} or Pt^{4+}) and the formation of clusters or isolated metallic nanoparticles was not observed (Kappler, 1998, 2001; Cabot et al., 2000). In the aerosol pyrolysis method Pt is found to be present as Pt clusters either in a metallic or in an oxidized state on the surface of SnO_2 particles (Matko et al., 1999, 2002). In this case the best signals were observed for a Pt/Sn ratio close to 0.019 (Matko et al., 1999).

The drastic effect of the amount of platinum doping on sensing properties was investigated further at CO concentrations up to 1000 ppm (Figure 9, to eliminate consumption effects these tests were performed with one sensor in a chamber). Also here doping with 0.2 wt% platinum results in the highest sensor signals compared to pure tin dioxide followed by the sensor with a doping of 2.0 wt%. However, the sensor with 2.0 wt%

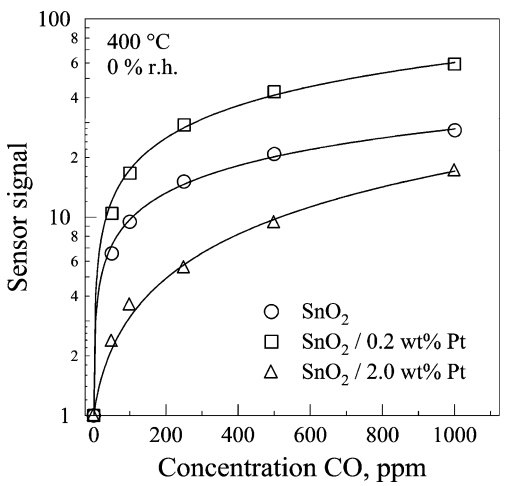

Figure 9. Sensor signal of differently doped sensors for different CO concentrations in dry air and at 400°C. SnO_2 with 0.2 wt% Pt (□, calibration function $S=1+1.245\times C^{0.56}$) shows higher sensor signals than pure SnO_2 (○, calibration function $S=1+0.918\times C^{0.49}$). SnO_2 with 2.0 wt% Pt (△, calibration function $S=1+0.038\times C^{0.88}$) shows the lowest sensor signals. This effect becomes smaller with increasing CO concentration. The measurements were performed with one sensor in the chamber.

platinum is becoming more and more sensitive and the large difference in sensitivity becomes less at higher concentrations. The sensor signal can be approximated by a power law with respect to the CO concentration, i.e. $S = 1 + aC_{CO}^{b}$. However, Figure 9 clearly indicates a different behavior for 2.0 wt% platinum doping compared to pure tin oxide and 0.2 wt% Pt doping, respectively. This can be quantified by: the pre-factor (i.e. a in $S = 1 + aC_{CO}^{b}$) of the power law fit which is 0.918, 1.245, and 0.038 for 0.0, 0.2, and 2.0 wt%, respectively, and by the power law exponent (i.e. b in $S = 1 + aC_{CO}^{b}$) of the power law fit which is 0.49, 0.56, and 0.88 for 0.0, 0.2, and 2.0 wt%, respectively. The pre-factor is more than one order of magnitude different for the 2.0 wt% platinum doping compared to the other sensors and the power law exponent also significantly changes. The latter fact indicates a change in the type of reactive oxygen species involved in the reaction with CO (Barsan & Weimar, 2001). At the operation temperature more than one oxygen species can be present at the surface and their relative concentration could depend on the presence and amount of noble metal.

Although the effect of the amount of platinum doping on SnO_2 sensing properties is large, no significant difference in oxidation/chemical state of platinum on SnO_2 has been observed for 0.2 and 2.0 wt% Pt, respectively. To summarize, only surface sensitive or element-specific methods such as XPS and EXAFS reveal information about the platinum functionalization. These methods revealed in both cases the presence of an oxidized form of platinum but show also a higher dispersion in the case of 0.2 wt% Pt (smaller clusters). The absence of charging effects for the platinum doped samples further indicates an embedding of the platinum within the tin dioxide lattice (see also the comparison of the resistance measurements in Figure 11).

The detailed mechanism of CO detection by tin dioxide in the presence of platinum on its surface has not been clarified yet. The effect of platinum doping on sensor sensitivity is usually described by two mechanisms; the spill-over or catalytic effect and Fermi energy control. In case of spill-over effect, CO oxidation can be accelerated because of the activation, i.e. dissociation, of oxygen on platinum. Then the activated oxygen species reach the SnO_2, where the final reaction with CO takes place. This results in shorter response time and larger sensitivity. This mechanism is generally accepted for Pt-doped SnO_2 gas sensors (Yamazoe, 1991). However, in the literature on catalytic low-temperature CO oxidation on 0.2–2.0 wt% Pt-impregnated SnO_2, a different mechanism, i.e. dissociative adsorption of oxygen on SnO_2 followed by oxygen reverse spillover from the SnO_2 onto Pt sites in isolated Pt-clusters and reaction with the CO chemisorbed on the Pt metal, is generally accepted since the works of Boulahouache et al. (1992) and Grass and Lintz (1995, 1997a, b). In this case (Fermi energy control) the electronic contact between SnO_2 and the noble metal particle influences the electrical resistance (conductance) of the sensors (Matsushima et al., 1988; Yamazoe, 1991). At equilibrium, the Fermi level of the catalyst and the semiconductor are at the same energy. The stoichiometry of the catalytically active noble metal particle/center (i.e. Pt or PtO_{2-X}) hereby depends on the composition of the ambient gas atmosphere and so does the position of its Fermi level. Consequently, the position of the Fermi level of SnO_2 and therefore the concentration of charge carriers (i.e. electrical resistance or conductance) will be influenced by surface reactions on the catalyst. This effect, i.e. change in stoichiometry and chemical state of the platinum center (i.e. Pt or PtO_{2-X}) on SnO_2 sensors, has been recently observed and proved by *in situ* EXAFS analysis (Gaidi et al., 1998, 2000).

The low signals to CO of the sensors with the high platinum loading (2.0 wt%) may result from "localized" CO consumption without electron transfer to the conduction band of SnO_2. In this case Pt acts as a "good catalyst" and catalytic oxidation of carbon monoxide takes place locally on platinum. In this case the charge transfer occurs only in a localized manner and has no direct impact on the electrical conduction of SnO_2. In order to validate this hypothesis, the analyte gas containing CO was introduced first to an isolated sensor in a confined measuring volume (position #1) and subsequently to a second measuring volume where the sensors were arranged in subsequent directions of the flow (position #2 to #5) with two sensors opposing each other (a, b). For this experiment 8 identical sensors were fabricated and simultaneously tested. Figure 10 shows the sensor response for 0.2 wt% platinum doping (left) and 2.0 wt% platinum doping (right). The

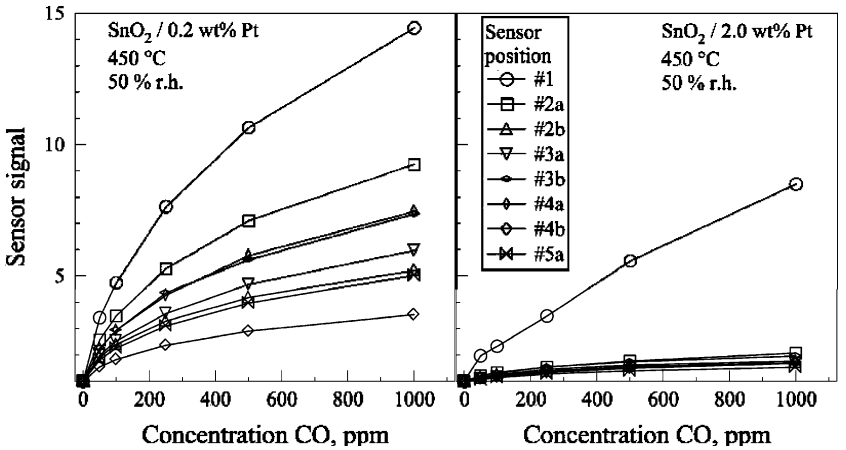

Figure 10. Sensor signal of SnO_2 with 0.2 wt% Pt (left) and SnO_2 with 2.0 wt% Pt (right) for different CO concentrations. In both measurements, two test chambers are connected in series, the first one containing a single sensor (#1) and the second one containing seven sensors (#2a to #5a). For 0.2 wt% Pt, the Sensor signal decreases subsequently in the direction of the gas flow. For 2.0 wt% Pt, only the single sensor (#1) shows sensor signals, whereas all sensors in the second chamber show almost no sensor signals. The measurements have been performed at 450°C and in 50% relative humidity.

first sensor (position #1) shows the highest signals followed by the sensors in the second chamber. In the second chamber a decrease of sensor signal at increasing downstream position is evident (Figure 10, left). All sensors with 0.2 wt% platinum doping have a remarkable sensitivity for CO even at a reduced CO concentration because of its consumption at upstream sensors. Please note in comparison to previous data, that the consumption measurements were performed at 50% r.h. and therefore show slightly smaller signals towards CO. The situation is rather different when increasing the platinum doping from 0.2 to 2.0 wt% (figure 10, right). In this case only the first sensor is responding to CO, however, with much lower signals as for 0.2 wt% platinum doping. All other downstream sensors are almost not sensitive towards CO even at high CO concentrations.

The drastic reduction in CO signal for "downstream" sensors with high platinum loading (2.0 wt%) indicates higher CO consumption on them. It leads to the decrease in effective CO concentration (which is seen by sensors), and therefore to the drastic decrease in the sensor signals because of the non-linear sensor response (i.e. power law dependence on the CO concentration, e.g. see Figures 4, 8 and 9). It should be noted that higher platinum loadings resulted in low platinum dispersion (XPS, Table 1) and usually, flame-made materials with higher Pt-content result in an easier reduction of platinum at higher loading (evidenced by EXAFS (Stark et al., 2005)). Therefore, the "localized" CO consumption without electron transfer to the conduction band of SnO_2 is likely. However, this can be regarded only as a hypothesis and additional investigations are necessary. In general, a direct correlation between the sensing properties of Pt doped SnO_2 with their catalytic (i.e. "CO consumption") properties is desirable but rather difficult. Recent studies also indicated that the influence of the substrate, heater (on the back side of the sensor substrate) and boundaries between oxide, Pt-electrodes and sensor substrate cannot be neglected making the situation even more complex (Kappler, 2001; Kappler et al., 2001; Barsan & Weimar, 2003).

Stability of gas sensors

The sensors were tested for 20 days while every second day the sensors were exposed to three different CO concentrations (i.e. to 10, 240 and 50 ppm) which were separated by 3 h. These tests were performed on two identical sensor pairs of pure SnO_2 and doped with 0.2 wt% Pt placed symmetrically into two chambers each. Figure 11 shows the response of all four sensors. Identical sensors showed nearly identical resistance which indicates the high reproducibility. The platinum

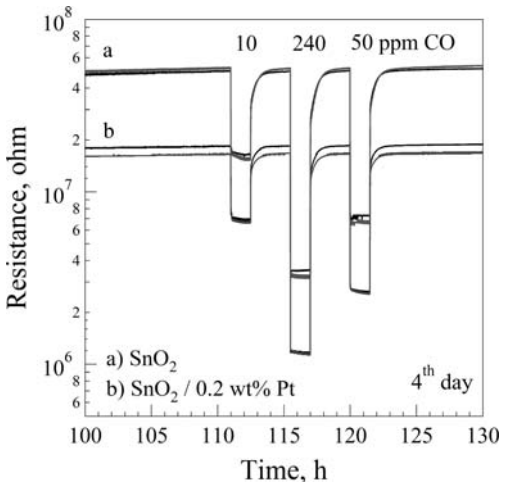

Figure 11. Resistance of two identical pairs of SnO_2 sensors (a) and (b) with 0.2 wt% Pt during exposure to three different CO concentrations (10, 240 and 50 ppm) shown for the 4th day of a 20 days period. All sensors return to zero setting upon end of the exposure showing excellent reproducibility and stability.

doped SnO_2 sensors have lower resistance than pure SnO_2 which might be beneficial for the final device. These results are corroborated by the XPS analysis which showed a higher charging of the pure SnO_2 sample. All sensors recover to their initial resistance once the CO concentration is back to zero. However, a small increase of the overall resistance at 0 ppm CO over time is observed. This small drift is less pronounced for the platinum doped sensor because of the surface stabilization effect of platinum in the presence of CO. The stability of the platinum doped sensors is better than the undoped tin dioxide because the absorption/desorption equilibrium is reached faster. This is further corroborated by the fact that essentially no drift has been observed at the presence of CO (Figure 12). The high stability of the sensors derived from flame-made powders becomes evident when comparing with sol-gel derived powders under the same conditions. This may be because of the high dispersion in the matrix and the well-crystalline nature of the flame-made materials. The sol-gel-made powder drifts steadily over the entire time period which was evaluated (20 days) (Kappler, 2001).

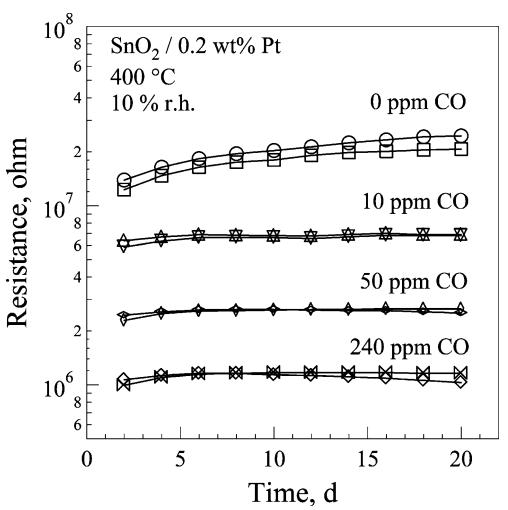

Figure 12. Resistance of SnO_2/0.2 wt% Pt sensors over 20 days in air and in 10, 50 and 240 ppm CO. The measurement was performed at 400°C and in 10% relative humidity. Excellent reproducibility and stability is observed over that period and CO concentration.

Summary and Conclusions

Gas sensors made from tin dioxide nanoparticles have been investigated for CO detection. Sensor characteristics were directly controlled by adjusting nanoparticle properties such as grain size and platinum functionalization. Here, flame spray pyrolysis (FSP) was used to synthesize in one step SnO_2 nanoparticles pure or Pt-doped with controlled particle size and platinum content. Sensors made from SnO_2 particles with a grain size of 10 nm show a 5 times higher sensor signal than particles of 20 nm and more than one order higher sensor signal than sensors made from 330 nm particles. The particle size control afforded by FSP can be directly used to tune sensor performance without post-treatment of the sensing material. *In situ* functionalization (one-step) by doping with platinum during FSP synthesis resulted in more sensitive sensors when containing 0.2 wt% Pt rather than 2.0 wt%. The latter showed a detrimental effect because of the catalytic conversion of CO without electron transfer. CO consumption measurements and detailed structural analysis using XPS and EXAFS showed that Pt is incorporated as oxidized clusters. These oxidized platinum clusters were slightly reduced in vacuum during the XPS analysis. Furthermore, a low Pt concentration (0.2 wt%) seems to lead to a higher dispersion of Pt. The stability of the

sensors was tested and found suitable for low level CO detection: <10 ppm according to European legislation and 50 according to US.

Acknowledgments

We would like to thank Dr. Frank Krumeich for providing the HRTEM, STEM and EDX analyses and Dr. Stefan Mangold for assistance in using beam line ANKA-XAS and the fluorescence detection at the Synchrotron Radiation Facility ANKA of Forschungszentrum Karlsruhe. The EXAFS studies were supported within the project XAS_03_030 by the European Community-Research Infrastructure Action under the FP6: "Structuring the European Research Area". (Integrating Activity on Synchrotron and Free Electron Laser Science (IA-SFS) RII3-CT-2004-506008).

References

Barsan N., M. Schweizer-Berberich & W. Gopel, 1999. Fundamental and practical aspects in the design of nanoscaled SnO_2 gas sensors: a status report. Fres. J. Anal. Chem. 365(4), 287–304.

Barsan N. & U. Weimar, 2001. Conduction model of metal oxide gas sensors. J. Electroceram. 7(3), 143–167.

Barsan N. & U. Weimar, 2003. Understanding the fundamental principles of metal oxide based gas sensors; the example of CO sensing with SnO_2 sensors in the presence of humidity. J. Phys. Cond. Matter 15(20), R813–R839.

Bazin D., H. Dexpert, J. Lynch & J.P. Bournonville, 1999. XAS of electronic state correlations during the reduction of the bimetallic $PtRe/Al_2O_3$ system. J. Synchr. Rad. 7, 465.

Bolzan A.A., C. Fong, B.J. Kennedy & C.J. Howard, 1997. Structural studies of rutile-type metal dioxides. Acta Crystall. Section B – Struct. Sci. 53(3), 373–380.

Boulahouache A., G. Kons, H.G. Lintz & P. Schulz, 1992. Oxidation of carbon-monoxide on platinum tin dioxide catalysts at low-temperatures. Appl. Catal. – Gen. 91(2), 115–123.

Cabot A., 2004. Influence of Catalytic Additives on Metal Oxide Nanoparticles for Gas Sensing Applications. Barcelona: Universitat de Barcelona.

Cabot A., J. Arbiol, J.R. Morante, U. Weimar, N. Barsan & W. Gopel, 2000. Analysis of the noble metal catalytic additives introduced by impregnation of as obtained SnO_2 sol-gel nanocrystals for gas sensors. Sensors Actuators B – Chemical 70(1–3), 87–100.

Cabot A., A. Dieguez, A. Romano-Rodriguez, J.R. Morante & N. Barsan, 2001. Influence of the catalytic introduction procedure on the nano- SnO_2 gas sensor performances – where and how stay the catalytic atoms?. Sensors Actuators B – Chemical 79(2–3), 98–106.

Cabot A., A. Vila & J.R. Morante, 2002. Analysis of the catalytic activity and electrical characteristics of different modified SnO_2 layers for gas sensors. Sensors Actuators B – Chemical 84(1), 12–20.

Cheary R.W. & A.A. Coelho, 1998. Axial divergence in a conventional X-ray powder diffractometer. I. Theoretical foundations. J. Appl. Crystallogr. 31, 851–861.

Dieguez A., A. Vila, A. Cabot, A. Romano-Rodriguez, J.R. Morante, J. Kappler, N. Barsan, U. Weimar & W. Gopel, 2000. Influence on the gas sensor performances of the metal chemical states introduced by impregnation of calcinated SnO_2 sol-gel nanocrystals. Sensors Actuators B – Chemical 68(1–3), 94–99.

EN. 2000. Directive 2000/69/EC of the European parliament and of the council. Official Journal of the European Commission, L313/12.

Eranna G., B.C. Joshi, D.P. Runthala & R.P. Gupta, 2004. Oxide materials for development of integrated gas sensors – a comprehensive review. Crit. Rev. Solid State Mat. Sci. 29(3–4), 111–188.

Gaidi M., J.L. Hazemann, I. Matko, B. Chenevier, M. Rumyantseva, A. Gaskov & M. Labeau, 2000. Role of Pt aggregates in Pt/SnO_2 thin films used as gas sensors – investigations of the catalytic effect. J. Electrochem. Soc. 147(8), 3131–3138.

Gaidi M., M. Labeau, B. Chenevier & J.L. Hazemann, 1998. In-situ EXAFS analysis of the local environment of Pt particles incorporated in thin films of SnO_2 semi-conductor oxide used as gas-sensors. Sensors Actuators B – Chemical 48(1–3), 277–284.

Grandjean D., R.E. Benfield, C. Nayral, A. Maisonnat & B. Chaudret, 2004. EXAFS and XANES Study of a Pure and Pd Doped Novel Sn/SnO_x nanomaterial. J. Phys. Chem. B 108(26), 8876–8887.

Grass K. & H.G. Lintz, 1995. Tin(IV)oxide supported noble metal catalysts for the carbon monoxide oxidation at low temperatures. Preparation of Catalysts VI: Studies in surface science and catalysis, Elsevier Science Publ., Amsterdam, pp. 1111–1119.

Grass K. & H.G. Lintz, 1997a. The kinetics of carbon monoxide oxidation on tin(IV) oxide supported platinum catalysts. J. Catal. 172(2), 446–452.

Grass K. & H.G. Lintz, 1997b. Oxidation of carbon monoxide over platinum–tin(IV) oxide catalysts: an example of spill-over catalysis?. Spillover Migration Surface Species on Catalysts 112, 135–142.

Grunwaldt J.D., U. Gobel & A. Baiker, 1997. Preparation and characterization of thin TiO_2-films on gold/mica. Fres. J. Anal. Chem. 358(1–2), 96–100.

Iwasawa Y. 1996. Characterization and Chemical Design of Oxide Surfaces. 11th International Congress on Catalysis, Baltimore, pp. 21–34.

Johannessen T. & S. Koutsopoulos, 2002. One-step flame synthesis of an active Pt/TiO_2 catalyst for SO_2 oxidation – a possible alternative to traditional methods for parallel screening. J. Catal. 205(2), 404–408.

Kappen P., L. Tröger, G. Materlik, C. Reckleben, K. Hansen, J.-D. Grunwaldt & B.S. Clausen, 2002. Silicon drift detectors as a tool for time-resolved fluorescence XAFS on low-concentrated samples in catalysis. J. Sync. Rad. 9, 246–253.

Kappler J., 2001. Characterization of high-performance SnO_2 gas sensors for CO detection by *in situ* techniques. Aachen: Saker Verlag.

Kappler J., N. Barsan, U. Weimar, A. Dieguez, J.L. Alay, A. Romano-Rodriguez, J.R. Morante & W. Gopel, 1998. Correlation between XPS, Raman and TEM measurements and the gas sensitivity of Pt and Pd doped SnO_2 based gas sensors. Fres. J. Anal. Chem. 361(2), 110–114.

Kappler J., A. Tomescu, N. Barsan & U. Weimar, 2001. CO consumption of Pd doped SnO_2 based sensors. Thin Solid Films 391(2), 186–191.

Kim K.S., N. Winograd & R.E. Davis, 1971. Electron spectroscopy of platinum-oxygen surfaces and application to electrochemical studies. J. Am. Chem. Soc. 93(23), 6296–6297.

Mädler L., H.K. Kammler, R. Mueller & S.E. Pratsinis, 2002a. Controlled synthesis of nanostructured particles by flame spray pyrolysis. J. Aerosol Sci. 33(2), 369–389.

Mädler L. & S.E. Pratsinis, 2002. Bismuth oxide nanoparticles by flame spray pyrolysis. J. Am. Ceramic Soc. 85(7), 1713–1718.

Mädler L., W.J. Stark & S.E. Pratsinis, 2002b. Flame-made ceria nanoparticles. J. Mater. Res. 17(6), 1356–1362.

Mädler L., W.J. Stark & S.E. Pratsinis, 2003. Simultaneous deposition of Au nanoparticles during flame synthesis of TiO_2 and SiO_2. J. Mater. Res. 18(1), 115–120.

Matko I., M. Gaidi, B. Chenevier, A. Charai, W. Saikaly & M. Labeau, 2002. Pt doping of SnO_2 thin films – a transmission electron microscopy analysis of the porosity evolution. J. Electrochem. Soc. 149(8), H153–H158.

Matko I., M. Gaidi, J.L. Hazemann, B. Chenevier & M. Labeau, 1999. Electrical properties under polluting gas (CO) of Pt- and Pd-doped polycrystalline SnO_2 thin films: analysis of the metal aggregate size effect. Sensors Actuators B – Chemical 59(2–3), 210–215.

Matsushima S., Y. Teraoka, N. Miura & N. Yamazoe, 1988. Electronic interaction between metal additives and tin dioxide in tin dioxide-based gas sensors. Jap. J. Appl. Phys., Part 1: Regular Papers, Short Notes & Review Papers 27(10), 1798–1802.

Muilenberg G.E., 1979. Handbook of Photoelectron Spectroscopy. Eden Prairie, Minnesota: Perkin-Elmer Corp.

Pearce T.C., S.S. Schiffman, H.T. Nagle & J.W. Gardner,. 2004. Handbook of Machine Olfaction: Electronic Nose Technology. Weinheim: Wiley-VCH Verlag GmbH.

Ressler T., 1998. WinXAS: a program for X-ray absorption spectroscopy data analysis under MS-Windows. J. Synchr. Rad. 5, 118.

Rothschild A. & Y. Komem, 2004. The effect of grain size on the sensitivity of nanocrystalline metal-oxide gas sensors. J. Appl. Phys. 95(11), 6374–6380.

Sahm T., A. Gurlo, N. Barsan & U. Weimar, Properties of indium oxide semiconducting sensors deposited by different techniques. J. Particulate Sci. (submitted).

Sahm T., A. Gurlo, N. Bârsan, U. Weimar & L. Mädler, 2005. Fundamental studies on SnO_2 by means of simultaneous work function change and conduction measurements. Thin Solid Films 490(1), 43–47.

Sahm T., L. Mädler, A. Gurlo, N. Barsan, S.E. Pratsinis & U. Weimar, 2004. Flame spray synthesis of tin dioxide nanoparticles for gas sensing. Sensors Actuators B – Chemical 98(2–3), 148–153.

Schweizer-Berberich M., J.G. Zheng, U. Weimar, W. Gopel, N. Barsan, E. Pentia & A. Tomescu, 1996. The effect of Pt and Pd surface doping on the response of nanocrystalline tin dioxide gas sensors to CO. Sensors Actuators B – Chemical 31(1–2), 71–75.

Stark W.J., J.-D. Grunwaldt, M. Maciejewski, S.E. Pratsinis & A. Baiker, 2005. Improved thermal stability of flame-made pt/ceria/zirconia for low-temperature oxygen exchange. Chem. Mat. 17, 3352–3359.

Strobel R., W.J. Stark, L. Mädler, S.E. Pratsinis & A. Baiker, 2003. Flame-made platinum/alumina: structural properties and catalytic behaviour in enantioselective hydrogenation. J. Catal. 213(2), 296–304.

Tani T., L. Mädler & S.E. Pratsinis, 2002. Homogeneous ZnO nanoparticles by flame spray pyrolysis. J. Nanoparticle Res. 4(4), 337–343.

Xu C., J. Tamaki, N. Miura & N. Yamazoe, 1991. Grain-size effects on gas sensitivity of porous SnO_2-based elements. Sensors Actuators B – Chemical 3(2), 147–155.

Yamazoe N., 1991. New approaches for improving semiconductor gas sensors. Sensors Actuators, B: Chemical B 5(1–4), 7–19.

Yang J.C., Y.C. Kim, Y.G. Shul, C.H. Shin & T.K. Lee, 1997. Characterization of photoreduced Pt/TiO_2 and decomposition of dichloroacetic acid over photoreduced Pt/TiO_2 catalysts. Appl. Surf. Sci. 121, 525–529.